

Mean-field analysis of collapsing and exploding Bose-Einstein condensates

Hiroki Saito and Masahito Ueda

Department of Physics, Tokyo Institute of Technology, Tokyo 152-8551, Japan

(Dated: October 27, 2018)

The dynamics of collapsing and exploding trapped Bose-Einstein condensates caused by a sudden switch of interactions from repulsive to attractive are studied by numerically integrating the Gross-Pitaevskii equation with atomic loss for an axially symmetric trap. We investigate the decay rate of condensates and the phenomena of bursts and jets of atoms, and compare our results with those of the experiments performed by E. A. Donley *et al.* [Nature **412**, 295 (2001)]. Our study suggests that the condensate decay and the burst production is due to local intermittent implosions in the condensate, and that atomic clouds of bursts and jets are coherent. We also predict nonlinear pattern formation caused by the density instability of attractive condensates.

I. INTRODUCTION

Bose-Einstein condensates (BECs) of trapped atomic vapor have been realized in several atomic species [1, 2, 3, 4, 5, 6]. One of the remarkable features of these systems is that both strength [7] and sign [8, 9, 10] of interactions between atoms can be tuned by adjusting an external magnetic field near a Feshbach resonance [11]. This has opened up the possibility to study collapsing and exploding BECs in a controllable manner, thereby offering a stringent test of the Gross-Pitaevskii mean-field theory [12].

A trapped BEC with attractive interactions may be formed [13] when quantum pressure arising from Heisenberg's uncertain principle counterbalances the attractive force between atoms. This is possible when the parameter defined by $k \equiv N_0|a|/d_0$ is below a critical value k_{cr} , where N_0 is the number of BEC atoms, a the s-wave scattering length, and d_0 the size of the ground-state wave function of a harmonic trap. When the parameter k exceeds k_{cr} , attractive force dominates quantum pressure, causing BEC to collapse. In the experiments performed by a Rice group [14, 15, 16], BEC atoms are continuously supplied from a supercooled thermal gas, and collapse and growth cycles of BEC have been observed [16]. In the experiments performed at JILA [8, 9, 10], in contrast, N_0 is fixed and $a (< 0)$ is decreased by using the Feshbach resonance so as to meet the condition $k > k_{\text{cr}}$. This technique enabled them to determine the value of k_{cr} [9], and to observe exploding atomic ejection from collapsing BEC [8, 10], a phenomenon called “Bosenova” whose origin is currently under controversy [17, 18, 19, 20].

The Gross-Pitaevskii (GP) equation [12] has widely been used to study mean-field properties of BECs, offering fairly good quantitative account of a rich variety of experiments for repulsive BECs [21]. In the case of the attractive BECs, however, it is by no means clear to what extent mean-field theory is valid, for the attractive interaction might enhance many-body quantum correlations. In fact, a measured value of k_{cr} [9] is significantly smaller than that predicted by a mean-field theory [13, 22], the origin of the discrepancy being not yet understood.

The recent quantitative measurements on collapsing

and exploding BEC reported in Ref. [10] have motivated us to investigate to what extent mean-field theory can explain the experimental observations. This is the main purpose of this paper. By numerically integrating the GP equation with atomic loss, we show that the phenomena reported in Ref. [10], such as decay of condensates, ejection and refocus of atomic bursts, and jet formation, are reproduced by our numerical simulations. In addition, we predict that various patterns in atomic density are formed in the course of collapse.

This paper is organized as follows. Section II briefly reviews the GP equation with atomic loss due to inelastic collisions and describes the method of analysis of our simulations. Section III reports our results of numerical simulations using the GP equation, and compares them with the experimental data of Ref. [10]. Section IV provides the summary of this paper.

II. THE GROSS-PITAEVSKII EQUATION WITH ATOMIC LOSS AND METHODS OF ANALYSIS

The GP equation describes unitary time evolution of a macroscopic “wave function” ψ , and conserves the total number of atoms $\int |\psi|^2 d\mathbf{r}$. In reality, however, atoms are lost from the trap due to the two-body dipolar and three-body recombination losses. These effects may be taken into account by incorporating in the GP equation the imaginary terms describing these inelastic processes [17]:

$$i\hbar \frac{\partial}{\partial t} \psi = -\frac{\hbar^2}{2m} \nabla^2 \psi + V_{\text{trap}}(\mathbf{r})\psi + \frac{4\pi\hbar^2 a}{m} |\psi|^2 \psi - \frac{i\hbar}{2} (K_2 |\psi|^2 + K_3 |\psi|^4) \psi, \quad (1)$$

where V_{trap} is the trapping potential, and K_2 and K_3 denote two-body dipolar and three-body recombination loss-rate coefficients, respectively. The imaginary terms in Eq. (1) are phenomenologically introduced in order to take account of the fact that the two-body and three-body losses are proportional to the square and cube of the atomic density:

$$\frac{\partial}{\partial t} \int |\psi|^2 d\mathbf{r} = - \int (K_2 |\psi|^4 + K_3 |\psi|^6) d\mathbf{r}. \quad (2)$$

We assume that the atoms and molecules produced by inelastic collisions escape from the trap without affecting the condensate. The constants K_2 and K_3 include Bose statistical factors $1/2!$ and $1/3!$, respectively, which are needed for BEC [23], and describe the loss rate per atom.

In the situations we consider the two-body loss can be ignored. The two-body and three-body loss rates are given by $R_2 \equiv K_2|\psi|^2$ and $R_3 \equiv K_3|\psi|^4$, and their ratio by $R_{23} \equiv R_2/R_3 = K_2/(K_3|\psi|^2)$. They have the relation $R_2R_{23} = K_2^2/K_3$, which is always $\lesssim 0.1 \text{ s}^{-1}$ for ^{85}Rb [24] and ^7Li [25]. When the density is low and $R_2 \sim R_3$, $R_2 \lesssim 0.1 \text{ s}^{-1}$. Then both two-body and three-body losses can be ignored since we shall consider the time scale of $\lesssim 10 \text{ ms}$. When the density is high, the three-body loss dominates the two-body loss, and thus the two-body loss becomes unimportant. In our numerical simulations we shall therefore ignore the two-body loss term in Eq. (1). All results presented below are not affected if the two-body loss is taken into account.

The three-body loss, in contrast, plays a crucial role in determining the collapsing dynamics of BEC. When implosion occurs, the atomic density becomes extremely high, and so does the three-body recombination rate, until it stops the growth of the density. The maximum density in the process of implosion is determined by K_3 and a [17, 18, 19]. The values of K_3 far from the Feshbach resonance have been measured for ^{87}Rb [26], ^{23}Na [27], and ^7Li [25], and they agree with theoretical predictions [28, 29, 30] within a factor of ten. Near the Feshbach resonance, however, complicated behaviors of K_3 are predicted [31], with no precise experimental data available [24].

We performed numerical integration of the GP equation (1) using a finite-difference method with the Crank-Nicholson scheme [13]. Since the peak density changes drastically during implosion [18, 19], we very carefully controlled the time step to avoid error propagation. Initially we prepared the ground-state wave function by the method in Ref. [32] for an initial s-wave scattering length a_{init} and an initial number of BEC atoms N_0 . At $t = 0$ the interaction is suddenly switched from $a_{\text{init}} \geq 0$ to $a_{\text{collapse}} < 0$, inducing collapse of the condensate. We use the parameters of ^{85}Rb and assume the same trap geometry (i.e. radial frequency $\omega_{\perp}/2\pi = 17.5 \text{ Hz}$ and axial frequency $\omega_z/2\pi = 6.8 \text{ Hz}$) as that used in Ref. [10].

In Ref. [10], atoms after the collapse are classified into three parts: remnant, burst, and missing atoms. The remnant BEC is a dense atomic cloud peaking around the center of the trap, and the burst is a dilute one that spreads broadly around the remnant BEC. In our simulations, we identify the remnant, burst, and missing atoms as follows. The one-dimensional density distributions defined by $\rho_{\text{axial}}(z) \equiv \int |\psi|^2 dx dy$ and $\rho_{\text{radial}}(r) \equiv \int |\psi|^2 dz$ show bimodal structures, one peaking at the center and the other spreading around it (an example is shown in Fig. 5b). We identify the former as the remnant and the latter as the burst, and determine the axial and radial coordinates, z_b and r_b , of the boundaries between

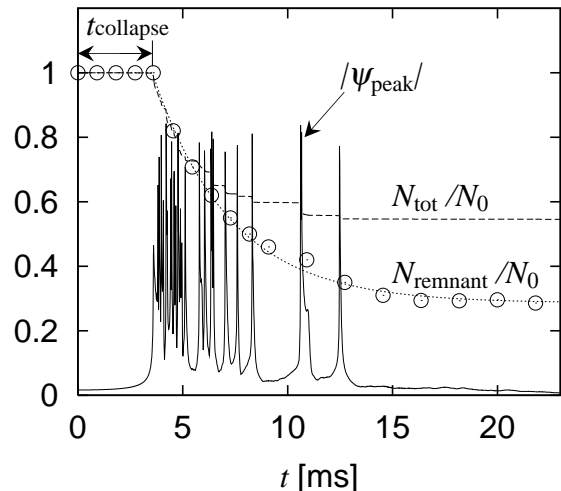


FIG. 1: Time evolutions of the peak height of the wave function $|\psi_{\text{peak}}|$ (solid curve in arbitrary scale), the fraction N_{tot}/N_0 of the total number of atoms remaining in the trap (dashed curve), and the fraction N_{remnant}/N_0 of the remnant BEC atoms (circles). The dotted curve is the best fit of the circles to Eq. (4) with $t_{\text{collapse}} = 3.6 \text{ ms}$ and $\tau_{\text{decay}} = 3.7 \text{ ms}$. At $t = 0$ the s-wave scattering length is changed from $a_{\text{init}} = 7a_0$ to $a_{\text{collapse}} = -30a_0$, where a_0 is the Bohr radius. The initial number of BEC atoms is $N_0 = 15000$, and the three-body recombination loss-rate coefficient is $K_3 = 2 \times 10^{-28} \text{ cm}^6/\text{s}$.

the remnant BEC and the burst. We then calculate the number of atoms in the remnant BEC as

$$N_{\text{remnant}} \equiv \int_0^{r_b} 2\pi r dr \int_{-z_b}^{z_b} dz |\psi|^2. \quad (3)$$

The burst atoms are defined by the ones outside the boundary. Because of ambiguities in defining the coordinates of the boundaries, N_{remnant} and N_{burst} defined this way have uncertainties of about $\pm 0.05N_0$, while the total number of atoms in the trap $N_{\text{tot}} \equiv N_{\text{remnant}} + N_{\text{burst}}$ is well defined. We define the number of missing atoms as $N_{\text{missing}} \equiv N_0 - N_{\text{tot}}$.

III. RESULTS OF NUMERICAL SIMULATIONS

A. Decay of the condensate and local intermittent implosions

We first study the situation in which the scattering length is switched from $a_{\text{init}} = 7a_0$ to $a_{\text{collapse}} = -30a_0$ at $t = 0$, where a_0 is the Bohr radius. Figure 1 shows time evolutions of the peak height $|\psi_{\text{peak}}|$ of the wave function, the total number of atoms in the trap N_{tot} , and the number of remnant BEC atoms N_{remnant} , where we assume $K_3 = 2 \times 10^{-28} \text{ cm}^6/\text{s}$.

Our numerical simulations show that the condensate first contracts slowly with its peak height $|\psi_{\text{peak}}|$ gradu-

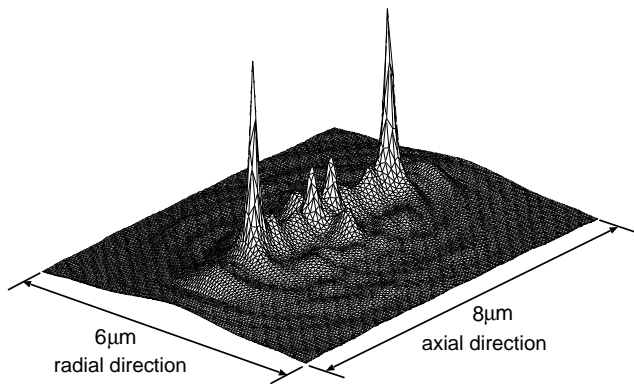


FIG. 2: A snapshot of the column density of the imploding BEC taken at 2.5 ms after the s-wave scattering length is changed from $a_{\text{init}} = 0$ to $a_{\text{collapse}} = -30a_0$. The initial number of BEC atoms is $N_0 = 15000$, and the loss-rate coefficient is $K_3 = 2 \times 10^{-28} \text{cm}^6/\text{s}$.

ally increasing. The total number of atoms remains constant during this process, since the recombination loss is negligible at such low densities. At $t \simeq 3.6$ ms, implosion suddenly occurs in a very localized region (the size of the density spike is $\sim 0.1 \mu\text{m}$ while the size of the BEC cloud is several micrometers) for a very short period of time (~ 0.1 ms). Furthermore the implosion occurs not just once but many times intermittently for about 10 ms [18, 19]. The three-body recombination loss prominently occurs during the implosion, since the atomic density becomes extremely high. Several tens of atoms are lost in each intermittent implosion, resulting in a step-wise decrease of N_{tot} . The decay of N_{remnant} is due to both three-body recombination and atomic burst ejection. We note that the behavior of N_{remnant} , shown as the plots in Fig. 1, is very similar to the experimental result (Fig. 1b of Ref. [10]).

The implosions occur not only at the center of the trap but also at other locations on the trap axis, and more than one density spike is often seen simultaneously. A snapshot of the imploding process with $a_{\text{init}} = 0$, $a_{\text{collapse}} = -30a_0$, and $N_0 = 15000$ is displayed in Fig. 2, where the image is taken 2.5 ms after the switch of interactions. Two large spikes are seen on the trap axis. In an isotropic trap, on the other hand, implosions always occur one by one at the center of the trap.

B. Collapse and decay times

The total number of atoms of the system remains constant for some time after the switch of interactions, and suddenly it begins to decay. We call the time at which the sudden decay begins ‘collapse time’ t_{collapse} (see Fig. 1). Since the collapse time is determined mainly by slow accumulation of atoms towards the center of the trap, t_{collapse} only weakly depends on the value of K_3 . In

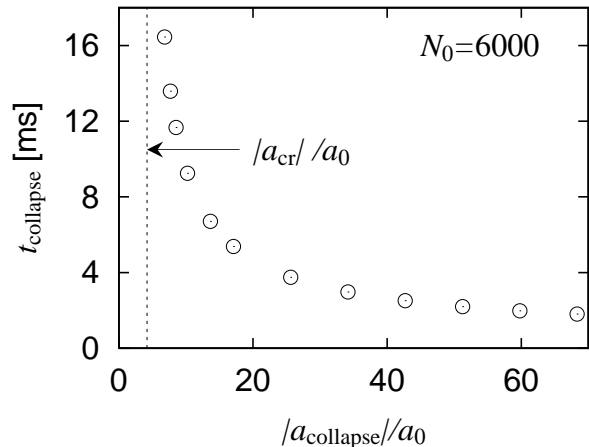


FIG. 3: The collapse time t_{collapse} at which implosions begin as a function of $|a_{\text{collapse}}|/a_0$, where the initial number of BEC atoms is $N_0 = 6000$. At $t = 0$ the s-wave scattering length is switched from $a_{\text{init}} = 0$ to $a_{\text{collapse}} < 0$. The dashed line indicates the critical ratio $|a_{\text{cr}}|/a_0$ for $N_0 = 6000$, below which the condensate does not collapse.

Fig. 1, $t_{\text{collapse}} = 3.6$ ms, which agrees with the experimental result of 3.7 ms [10]. Figure 3 shows the dependence of t_{collapse} on $|a_{\text{collapse}}|/a_0$, where $a_{\text{init}} = 0$ and $N_0 = 6000$ [33]. The plots are in good agreement with the experimental ones (Fig. 2 of Ref. [10]). For another set of parameters $a_{\text{init}} = 89a_0$ and $a_{\text{collapse}} = -15a_0$, we obtain $t_{\text{collapse}} = 15.9$ ms, which is also consistent with the experimental finding [10]. The collapse time increases for larger values of a_{init} , since the atomic cloud spreads more widely and therefore it takes longer time for the cloud to get to the center of the trap.

Fitting

$$N_{\text{remnant}}(t) = [N_0 - N_{\text{remnant}}(\infty)] e^{-\frac{t-t_{\text{collapse}}}{\tau_{\text{decay}}}} + N_{\text{remnant}}(\infty) \quad (4)$$

to the plots in Fig. 1 (dotted curve), we obtain the decay time constant $\tau_{\text{decay}} \simeq 3.7$ ms. For $a_{\text{init}} = 0$, and $N_0 = 6000$ and 15000 , τ_{decay} is almost the same as the above one, and for $a_{\text{collapse}} = -60a_0$ it becomes $\tau_{\text{decay}} \simeq 3.1$ ms which agrees reasonably well with the experimental finding of 2.8 ms [10].

C. Remnant, burst, and missing atoms

Figure 4a shows the fractions of remnant, burst, and missing atoms after the implosion has finished for $a_{\text{init}} = 0$ and $a_{\text{collapse}} = -30a_0$. We note that N_{remnant} is much larger than N_{cr} when N_0 is large, as observed experimentally [10]. To put it differently, once the condensate expands following the collapse, the critical density will not be reached even when $N_{\text{remnant}} > N_{\text{cr}}$. This is because the ratio ω_{\perp}/ω_z is irrational and therefore the axial

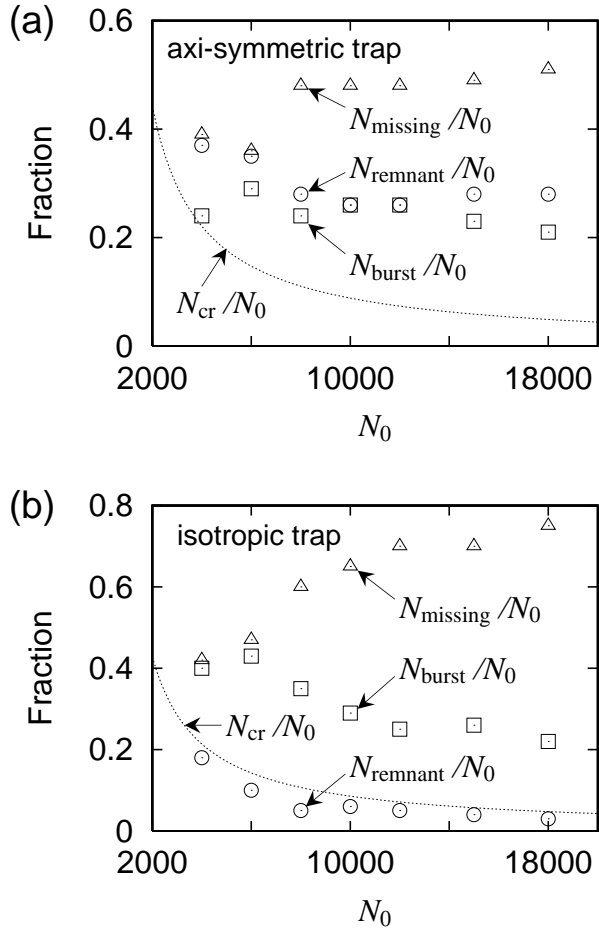


FIG. 4: The fractions of the remnant N_{remnant}/N_0 (circles), burst N_{burst}/N_0 (squares), and missing atoms N_{missing}/N_0 (triangles) after the collapse for (a) an axi-symmetric trap and (b) an isotropic trap, where N_0 is the initial number of BEC atoms. The dotted curves show the fraction N_{cr}/N_0 of the critical number of atoms. The s-wave scattering length is switched from $a_{\text{init}} = 0$ to $a_{\text{collapse}} = -30a_0$ with the loss-rate coefficient $K_3 = 2 \times 10^{-28} \text{ cm}^6/\text{s}$.

and radial refocuses of the burst atoms do not occur simultaneously, with no further implosions occurring.

This result presents a sharp contrast with that for an isotropic case shown in Fig. 4b, where the trap frequency is chosen to be the geometric mean $(\omega_{\perp}^2 \omega_z)^{1/3}$. The numbers of remnant atoms N_{remnant} are always below N_{cr} . This is because all collapsing atoms go to the center of the trap simultaneously, and therefore more implosions occur in an isotropic trap, which increases N_{missing} and decreases N_{remnant} . Moreover, the implosions occur also when the burst atoms refocus, since they concentrate at the center of the trap. The data in Fig. 4b are taken before the first refocus. Nevertheless, we note that N_{remnant} is already below N_{cr} .

We also note that in the axi-symmetric trap the fractions N_{remnant}/N_0 , N_{burst}/N_0 , and N_{missing}/N_0 are almost independent of N_0 , particularly for $N_0 > 6000$,

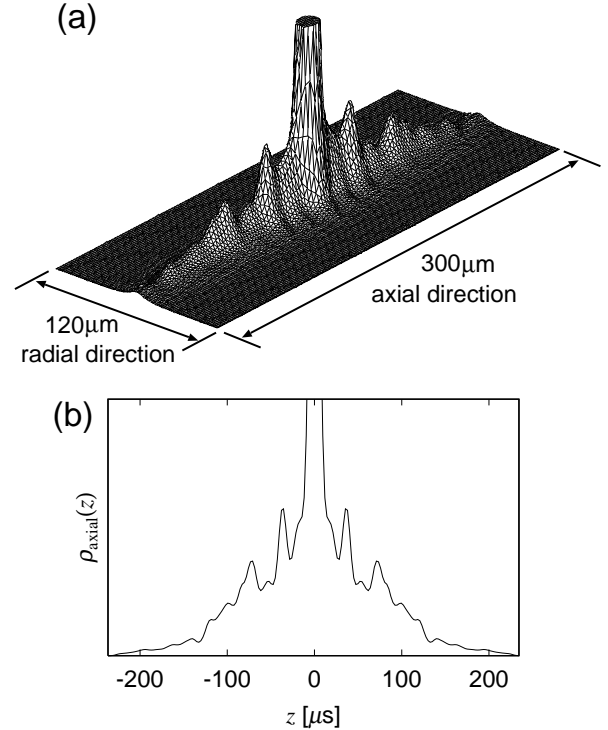


FIG. 5: (a) The integrated column density $\rho(x, z) = \int |\psi|^2 dy$ seen from the direction perpendicular to the trap axis and (b) the one-dimensional density distribution $\rho_{\text{axial}}(z) = \int |\psi|^2 dx dy$ along the axial direction. The s-wave scattering length is switched from $a_{\text{init}} = 0$ to $a_{\text{collapse}} = -30a_0$ with $K_3 = 2 \times 10^{-28} \text{ cm}^6/\text{s}$, where the images are taken at $t = 33.6$ ms. The images are smoothed in accordance with the experimental resolution ($7 \mu\text{m}$ FWHM), and the central peaks are truncated.

which is consistent with the experiments [10]. This is a consequence of the fact that the number of implosions occurring in the collapse is roughly proportional to N_0 and that the numbers of the burst and missing atoms in each implosion are almost constant.

D. Atomic bursts and “jets”

A burst atom cloud is usually too broadly spread and hence too dilute to be seen. However, at every π/ω_{\perp} (or π/ω_z) the cloud refocuses along the axial (or radial) direction and can be observed. Figure 5a shows the column density seen from the direction perpendicular to the trap axis and Fig. 5b shows the one-dimensional distribution $\rho_{\text{axial}}(z) \equiv \int |\psi|^2 dx dy$, when the burst atoms focus along the trap axis (corresponding to Fig. 3 of Ref. [10]). The s-wave scattering length is switched from $a_{\text{init}} = 0$ to $a_{\text{collapse}} = -30a_0$ at $t = 0$ and the image is taken at $t = 33.6 \text{ ms} \simeq t_{\text{collapse}} + \pi/\omega_{\perp}$. There are small peaks in the ridge of focus, which appear to correspond to the shoulders of the central peak in Fig. 3c of Ref. [10]. Ac-

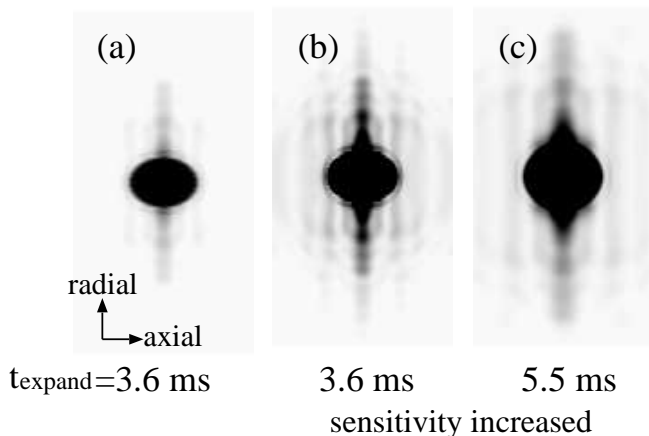


FIG. 6: The integrated column densities $\rho(x, z) = \int |\psi|^2 dy$ of condensates and jets seen from the radial direction. The wave function in Fig. 2 is expanded by a switch of the s-wave scattering length from $a_{\text{collapse}} = -30a_0$ to $a_{\text{expand}} = 100a_0$. The size of each image is $48 \times 90 \mu\text{m}$. (a) The image is taken with $t_{\text{expand}} = 3.6$ ms. (b) The sensitivity of imaging in (a) is increased. (c) The image is taken with $t_{\text{expand}} = 5.5$ ms and with the same sensitivity as (b).

cording to our theory the origin of the atomic burst is a release of kinetic energy of local spikes in the atomic density [17, 18, 19].

As regards the burst energy, it is at present difficult to compare our results with the experimental ones. One reason is that although the burst energy depends not only on a_{collapse} but also on K_3 [19], experimental values of K_3 as a function of a_{collapse} are not available. The uncertainty in the boundaries between the remnant BEC and the burst and that in Gaussian fitting of the burst profile (see Fig. 5b) give rise to large errors in numerically determining the burst “temperature”, which also make quantitative comparison between theory and experiment difficult. More work (both theoretical and experimental) needs to be done in order to clarify the situation.

In the experiments [10], prolonged atomic clouds called “jets” are observed in the radial direction when the collapse is interrupted by switching the interaction from attractive to repulsive. The jets are distinguished from the bursts in that the energy of the former is much lower than the latter and that the direction of the jets is purely radial. In Ref. [10], the origin of the jets is considered to be the highly anisotropic spikes in the atomic density.

We performed numerical simulations under situations similar to the experimental ones. The s-wave scattering length is switched from $a_{\text{init}} = 0$ to $a_{\text{collapse}} = -30a_0$ at $t = 0$, and changed to $a_{\text{expand}} = 100a_0$ at $t = 2.5$ ms (a snapshot before expansion is shown in Fig. 2). Figure 6 shows the gray-scale images of the integrated column density $\rho(x, z) = \int |\psi|^2 dy$ after a $t_{\text{expand}} = 3.6$ ms expansion in (a) and (b), and $t_{\text{expand}} = 5.5$ ms in (c). In the image (a), prolonged atomic clouds similar to the jets reported in Fig. 5 of Ref. [10] appear in the

radial direction (the main jet at the center and two tiny jets on either side of it). The images (b) and (c), where the sensitivity of the imaging is increased, show that the jets are interference fringes. The parallel fringe pattern is characteristic of the interference between waves emanating from two point sources [34]. In fact, there are two spikes in the atomic density that play the role of two point sources of matter waves in Fig. 2. We find that the spacing between the fringes is proportional to t_{expand} . This supports our interpretation, since the spacing between the fringes from two point sources is known to be given by ht_{expand}/md [34], where d is the distance between two point sources. In the experimental images in Ref. [10] (particularly in Figs. 5d-f), the jets seem to be ejected from the edge of the remnant condensate, where the density is too low to form the spikes, which also supports our interpretation that the jets are the consequence of interference. Thus, the experimental observations of jets indicate that atoms expanding from spikes are coherent, suggesting that the burst atoms are also coherent.

E. Pattern formation

We found in Ref. [18] that various patterns in the atomic density are formed in the collapse processes caused by a sudden switch of interactions from repulsive to attractive, the origin of the pattern formation being attributed to the self-focusing effect of the attractive systems. Here we predict that a similar pattern formation does occur in ^{85}Rb BEC for experimentally available parameters.

Figure 7 shows pattern formation in axi-symmetric traps, where $N_0 = 5 \times 10^4$, and the s-wave scattering length is switched from $a_{\text{init}} = 400a_0$ to $a_{\text{collapse}} = -310a_0$. The pancake-shape trap has the ratio $\omega_z/\omega_{\perp} = \sqrt{8}$ with the same geometric mean frequencies as the cigar-shape trap. In the cigar-shape trap the cylindrical shell structure is formed, and in the pancake-shape trap the layered structure is formed.

Figure 8 shows time evolution of the integrated column density $\rho(x, z) = \int |\psi|^2 dy$ for an isotropic trap, where N_0 , a_{init} , and a_{collapse} are the same as in Fig. 7. We see that the density fluctuations grow to form four concentric spherical shells at $t = 7.7$ ms, which move inwards and collapse one by one; then at $t = 11$ ms we see that a new shell is being formed

The resolution of the imaging system in Ref. [10] ($7 \mu\text{m}$ FWHM) is inadequate for observing the patterns in Figs. 7 and 8 (the spacing between the shells is $\sim 1 \mu\text{m}$). Expansion of BEC before imaging will blur out the pattern. In order to observe the pattern formation, therefore, we need to improve the *in situ* imaging method, or to use larger d_0 and $|a|$ to enlarge the pattern.

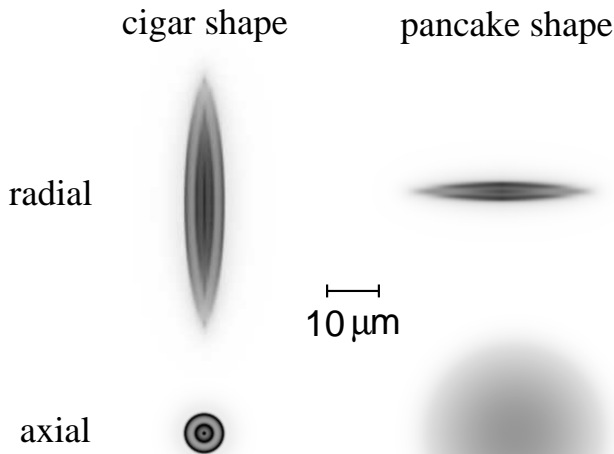


FIG. 7: Pattern formation in a cigar-shape trap (left panel) and a pancake-shape trap (right panel), where the column density is seen from the radial (upper images) and axial (lower images) directions. The initial number of atoms is $N_0 = 50000$, and at $t = 0$ the s-wave scattering length is switched from $a_{\text{init}} = 400a_0$ to $a_{\text{collapse}} = -310a_0$. The ratio is $\omega_z/\omega_\perp = 0.39$ ($\sqrt{8}$) with $\omega_\perp = 17.5$ Hz (9.03 Hz) in the cigar-shape (pancake-shape) trap, and the images are taken at $t = 6.2$ ms ($t = 4.8$ ms).

IV. SUMMARY

We have studied the dynamics of collapsing and exploding BECs by numerically solving the time-dependent GP equation with atomic loss (1), and compared our results with those of the experiments of Ref. [10]. We find that mean-field theory with atomic loss can account for the following experimental findings: (i) It takes the system a certain time t_{collapse} to undergo a sudden decrease in the number of atoms after the jump of a . (ii) The number of atoms in the condensate decays exponentially with a decay time constant of a few milliseconds. (iii) The burst atoms are ejected in the collapse process, and refocus after every half trap period. (iv) The fractions of remnant, burst, and missing atoms are almost independent of N_0 , and the number of remnant atoms is much larger than the critical number N_{cr} for large N_0 . (v) The jets are observed when the collapse is interrupted by jumping a to a positive value.

We have found that these phenomena are attributed to a rapid sequence of local intermittent implosions, and provided a new interpretation of the jets, i.e., the highly anisotropy of the jets is due to the interference fringes. This suggests that the burst atom cloud is coherent.

The validity of the mean-field GP equation is determined by the gas parameter na^3 , and the depletion is given by $\simeq (na^3)^{1/2}$. When the implosion occurs, $n|a|^3$ becomes $\sim 10^{-3}$ at the peak density in our simulations, which indicates that the mean-field approximation is still

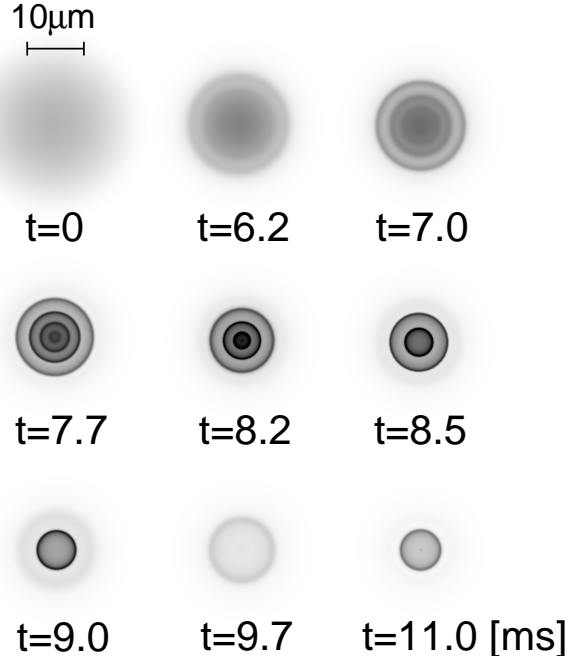


FIG. 8: Time evolution of the column density of BEC in an isotropic trap, where the trap frequency is $\omega/2\pi = 12.8$ Hz. At $t = 0$ the s-wave scattering length is switched from $a_{\text{init}} = 400a_0$ to $a_{\text{collapse}} = -310a_0$. The initial number of atoms is $N_0 = 50000$ and the loss-rate coefficient is $K_3 = 8 \times 10^{-26} \text{ cm}^6/\text{s}$.

valid at least qualitatively.

Our results presented here suggest that the mean-field approximation can be used to describe the collapsing and exploding dynamics at least qualitatively. A more quantitative comparison between experiments and numerical simulations might reveal effects beyond mean-field approximation. This possibility merits further experimental and theoretical study.

ACKNOWLEDGMENTS

We thank E. A. Donley for valuable comments. This work was supported by a Grant-in-Aid for Scientific Research (Grant No. 11216204) by the Ministry of Education, Science, Sports, and Culture of Japan, and by the Toray Science Foundation.

[1] M. H. Anderson, J. R. Ensher, M. R. Matthews, C. E. Wieman, and E. A. Cornell, *Science* **269**, 198 (1995).

[2] K. B. Davis, M. -O. Mewes, M. R. Andrews, N. J. van

- Druten, D. S. Durfee, D. M. Kurn, and W. Ketterle, Phys. Rev. Lett. **75**, 3969 (1995).
- [3] C. C. Bradley, C. A. Sackett, J. J. Tollett, and R. G. Hulet, Phys. Rev. Lett. **75**, 1687 (1995); **79**, 1170(E) (1997); C. C. Bradley, C. A. Sackett, and R. G. Hulet, *ibid.* **78**, 985 (1997).
- [4] D. G. Fried, T. C. Killian, L. Willmann, D. Landhuis, S. C. Moss, D. Kleppner, and T. J. Greytak, Phys. Rev. Lett. **81**, 3811 (1998).
- [5] A. Robert, O. Sirjean, A. Browaeys, J. Poupard, S. Nowak, D. Boiron, C. I. Westbrook, and A. Aspect, Science **292**, 461 (2001); F. P. D. Santos, J. Léonard, J. Wang, C. J. Barrelet, F. Perales, E. Rasel, C. S. Unnikrishnan, M. Leduc, and C. Cohen-Tannoudji, Phys. Rev. Lett. **86**, 3459 (2001).
- [6] G. Modugno, G. Ferrari, G. Roati, R. J. Brecha, A. Simoni, and M. Inguscio, Science **294**, 1320 (2001).
- [7] S. Inouye, M. R. Andrews, J. Stenger, H. -J. Miesner, D. M. Stamper-Kurn, and W. Ketterle, Nature **392**, 151 (1998).
- [8] S. L. Cornish, N. R. Claussen, J. L. Roberts, E. A. Cornell, and C. E. Wieman, Phys. Rev. Lett. **85**, 1795 (2000).
- [9] J. L. Roberts, N. R. Claussen, S. L. Cornish, E. A. Donley, E. A. Cornell, and C. E. Wieman, Phys. Rev. Lett. **86**, 4211 (2001).
- [10] E. A. Donley, N. R. Claussen, S. L. Cornish, J. L. Roberts, E. A. Cornell, and C. E. Wieman, Nature **412**, 295 (2001).
- [11] E. Tiesinga, A. J. Moerdijk, B. J. Verhaar, and H. T. C. Stoof, Phys. Rev. A **46**, R1167 (1992); E. Tiesinga, B. J. Verhaar, and H. T. C. Stoof, *ibid.* **47**, 4114 (1993).
- [12] E. P. Gross, Nuovo Cimento **20**, 454 (1961); J. Math. Phys. **4**, 195 (1963); L. P. Pitaevskii, Zh. Eksp. Teor. Fiz. **40**, 646 (1961) [Sov. Phys. JETP **13**, 451 (1961)]. See also A. J. Leggett, Rev. Mod. Phys. **73**, 307 (2001).
- [13] P. A. Ruprecht, M. J. Holland, K. Burnett, and M. Edwards, Phys. Rev. A **51**, 4704 (1995).
- [14] C. A. Sackett, C. C. Bradley, M. Welling, and R. G. Hulet, Appl. Phys. B **65**, 433 (1997).
- [15] C. A. Sackett, J. M. Gerton, M. Welling, and R. G. Hulet, Phys. Rev. Lett. **82**, 876 (1999).
- [16] J. M. Gerton, D. Strelakov, I. Prodan, and R. G. Hulet, Nature **408**, 692 (2000).
- [17] Yu. Kagan, A. E. Muryshev, and G. V. Shlyapnikov, Phys. Rev. Lett. **81**, 933 (1998).
- [18] H. Saito and M. Ueda, Phys. Rev. Lett. **86**, 1406 (2001).
- [19] H. Saito and M. Ueda, Phys. Rev. A **63**, 043601 (2001).
- [20] R. A. Duine and H. T. C. Stoof, Phys. Rev. Lett. **86**, 2204 (2001).
- [21] F. Dalfovo, S. Giorgini, L. P. Pitaevskii, and S. Stringari, Rev. Mod. Phys. **71**, 463 (1999).
- [22] A. Gammal, T. Frederico, and L. Tomio, Phys. Rev. A **64**, 055602 (2001).
- [23] Yu. Kagan *et al.*, JETP Lett. **42**, 209 (1985); H. T. C. Stoof, A. M. L. Janssen, J. M. V. A. Koelman, and B. J. Verhaar, Phys. Rev. A **39**, 3157 (1989).
- [24] J. L. Roberts, N. R. Claussen, S. L. Cornish, and C. E. Wieman, Phys. Rev. Lett. **85**, 728 (2000).
- [25] J. M. Gerton, C. A. Sackett, B. J. Frew, and R. G. Hulet, Phys. Rev. A **59**, 1514 (1999).
- [26] E. A. Burt, R. W. Ghrist, C. J. Myatt, M. J. Holland, E. A. Cornell, and C. E. Wieman, Phys. Rev. Lett. **79**, 337 (1997).
- [27] D. M. Stamper-Kurn, M. R. Andrews, A. P. Chikkatur, S. Inouye, H. -J. Miesner, J. Stenger, and W. Ketterle, Phys. Rev. Lett. **80**, 2027 (1998).
- [28] A. J. Moerdijk, H. M. J. M. Boesten, and B. J. Verhaar, Phys. Rev. A **53**, 916 (1996).
- [29] P. O. Fedichev, M. W. Reynolds, and G. V. Shlyapnikov, Phys. Rev. Lett. **77**, 2921 (1996).
- [30] B. D. Esry, C. H. Greene, and J. P. Burke, Jr., Phys. Rev. Lett. **83**, 1751 (1999).
- [31] E. Braaten and H. -W. Hammer, Phys. Rev. Lett. **87**, 160407 (2001).
- [32] M. Edwards, R. J. Dodd, C. W. Clark, and K. Burnett, J. Res. Natl. Inst. Stand. Technol. **101**, 553 (1996).
- [33] The similar results are obtained for a spherically symmetric trap and with different parameters in A. Eleftheriou and K. Huang, Phys. Rev. A **61**, 043601 (2000).
- [34] M. R. Andrews, C. G. Townsend, H. -J. Miesner, D. S. Durfee, D. M. Kurn, and W. Ketterle, Science **275**, 637 (1997).